RESEARCH ARTICLE

The fission yeast cytokinetic contractile ring regulates septum shape and closure

Sathish Thiyagarajan[1], Emilia Laura Munteanu[2], Rajesh Arasada[3], Thomas D. Pollard[3,4,5] and Ben O'Shaughnessy[6,*]

ABSTRACT

During cytokinesis, fission yeast and other fungi and bacteria grow a septum that divides the cell in two. In fission yeast closure of the circular septum hole by the β-glucan synthases (Bgs) and other glucan synthases in the plasma membrane is tightly coupled to constriction of an actomyosin contractile ring attached to the membrane. It is unknown how septum growth is coordinated over scales of several microns to maintain septum circularity. Here, we documented the shapes of ingrowing septum edges by measuring the roughness of the edges, a measure of the deviation from circularity. The roughness was small, with spatial correlations indicative of spatially coordinated growth. We hypothesized that Bgs-mediated septum growth is mechanosensitive and coupled to contractile ring tension. A mathematical model showed that ring tension then generates almost circular septum edges by adjusting growth rates in a curvature-dependent fashion. The model reproduced experimental roughness statistics and showed that septum synthesis sets the mean closure rate. Our results suggest that the fission yeast cytokinetic ring tension does not set the constriction rate but regulates septum closure by suppressing roughness produced by inherently stochastic molecular growth processes.

KEY WORDS: Septation, *Schizosaccharomyces pombe*, Cytokinesis, Mechanosensitivity, Cell wall growth

INTRODUCTION

Fungal and bacterial cells are enclosed by a cell wall whose growth is spatiotemporally regulated to maintain and evolve cell shape throughout the cell cycle (Cabib and Arroyo, 2013; Das et al., 2012; Pinho et al., 2013). Following cell division the fission yeast *S. pombe*, a rod-shaped fungus, elongates by growth at the rounded cell tips, whereas cell wall synthesis by the ovoid bacterium *Streptococcus pneumoniae* is largely confined to a region close to the division site and occurs during cell division (Pinho et al., 2013). The cell wall is a high modulus crosslinked network that withstands high turgor pressures and must be reshaped if the cell shape is to change. The mechanisms are debated, but growth is regulated by various signaling pathways in *S. pombe* (Das et al., 2012; Krapp and Simanis, 2008) and annealing of crosslinks is thought to assist local remodeling in the rod-shaped bacterium *E. coli* (Furchtgott et al., 2011). Mechanical effects

may also play a role. In *S. pombe*, network stretching by turgor pressure was proposed to locally promote the insertion of cell wall material (Drake and Vavylonis, 2013). Mechanical stress increases the rates of cell wall synthesis in *E. coli* (Amir et al., 2014), and the actin homologous protein MreB localizes to regions of negative curvature that define the sites of growth (Ursell et al., 2014).

Precise regulation of cell wall growth is essential for cell division, a process that results in two daughter cells that are properly enclosed by new cell wall. In fission yeast, and other fungi and bacteria, this is accomplished by growth of a septum in the central division plane during cytokinesis, the final stage of the cell cycle. Yeast grows a ~0.3 µm thick septum by centripetal growth of the almost circular inner septum edge that closes down the central septum hole over ~25 min, separating the cell (~3.7 µm in diameter) into two sealed compartments (Wu and Pollard, 2005) (Fig. 1A). Constriction of the septum is tightly coupled to constriction of an actomyosin contractile ring attached to the inside of the plasma membrane adjacent to the leading septum edge (Muñoz et al., 2013).

During septation, maintenance of the circularity of the growing septum edge ensures proper septum closure down to almost a point and encloses the daughter cells in new cell wall, but the regulating mechanism is unknown. For example, if the septum had an elongated shape it would close down to almost a slit.

The β-glucan synthases Bgs1p, Bgs2p, Bgs3p and Bgs4p, and the α-glucan synthase Ags1p that reside in the plasma membrane grow the septum (Cortés et al., 2005, 2007, 2012; Martín et al., 2003) (Fig. 1A). At the onset of constriction several thousand Bgs1p proteins participate at different locations around the edge (Arasada and Pollard, 2014; Cortés et al., 2007; Proctor et al., 2012). Given the intrinsic stochasticity of molecular complexes (Geertsema et al., 2014; Wang et al., 1998), independently operating Bgs1p molecules would presumably generate irregular edges; to maintain a smooth circular septum edge requires that growth rates are coordinated at locations that are up to ~4 µm apart. How the cell accomplishes this considerable technical challenge is unknown.

Several observations suggest that the yeast cytokinetic ring interacts with Bgs1p. The actomyosin ring is required for localization of Bgs1p into a compact band at the division site (Liu et al., 2002), and deletion of the IQ calmodulin-binding motifs from the ring component IQGAP Rng2p gives a uniform distribution of Bgs1p over the septum, in contrast to the distribution observed with wild-type, where Bgs1p is concentrated at the septum edge (Tebbs and Pollard, 2013). In mutants that contain reduced levels of the contractile ring protein Cdc15p, the ring slides along the membrane until ~2000 Bgs1p molecules are recruited to the membrane adjacent to the ring (Arasada and Pollard, 2014). Thus, the ring might influence septum growth, and mechanical interactions might play a role because the fission yeast ring has been reported to exert ~400 pN of tension (Stachowiak et al., 2014). Indeed, mutations of other ring components affect septation. Septa are abnormally thickened or incomplete when Myo2p is expressed at low

[1]Department of Physics, Columbia University, New York, NY 10027, USA.
[2]Department of Microbiology & Immunology, Columbia University College of Physicians and Surgeons, New York, NY 10032, USA. [3]Department of Molecular, Cellular, and Developmental Biology, Yale University, New Haven, CT 06520, USA. [4]Department of Molecular Biophysics and Biochemistry, Yale University, New Haven, CT 06520, USA. [5]Department of Cell Biology, Yale University, New Haven, CT 06520, USA. [6]Department of Chemical Engineering, Columbia University, New York, NY 10027, USA.

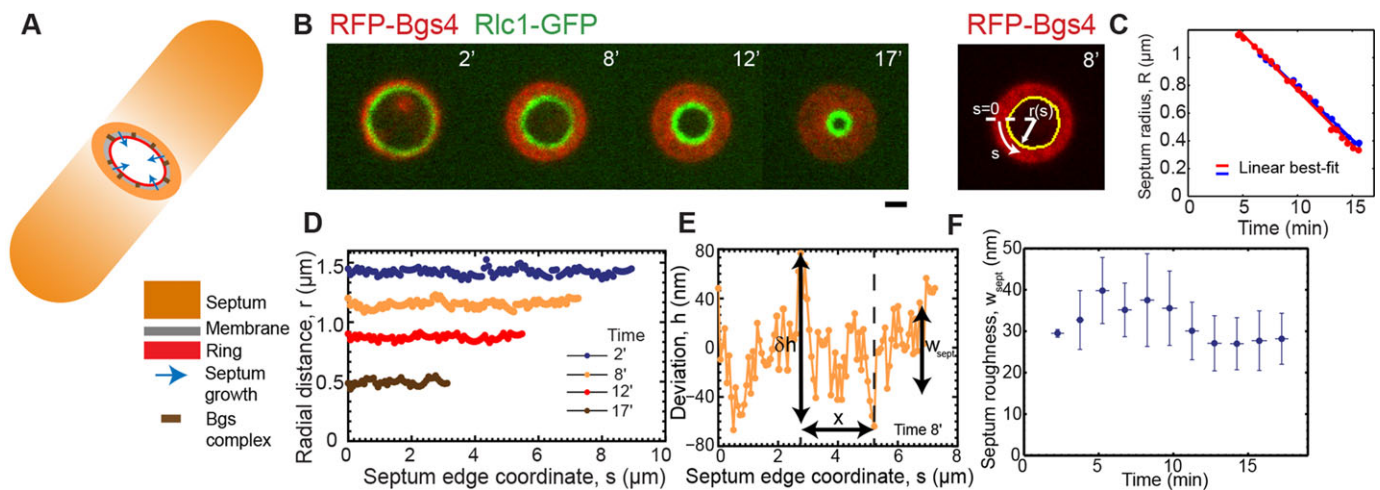*Author for correspondence (bo8@columbia.edu)

Fig. 1. Constricting septum edges in fission yeast are almost circular with low roughness. (A) Schematic of a *S. pombe* cell during cytokinesis, showing how constriction of the contractile ring and the septum edge are tightly coupled. The edge grows inwards as β-glucan synthases (Bgs) in the membrane synthesize the septum. (B) (left panel) Confocal fluorescence micrographs of division plane during constriction-septation of a yeast cell expressing RFP-Bgs4 and Rlc1-GFP (*t*=0 is the onset of septum growth). (Right panel) Edge determination (yellow) for the septum at 8 min. Scale bar: 1 µm. (C) Mean septum radii versus time for constrictions of two typical cells (blue and red). The best-fit straight lines have slopes of 75 nm/min (blue) and 80 nm/min (red). (D) Radial distance profile for each of the four septum edges in B. (E) Enlarged view of edge profile as shown in D (at 8 min) with details of deviation $h(s)$ of radial distance from mean value R. The roughness w of edges on a scale x quantifies the variations in edge radius on that scale δh. (F) Septum roughness versus time for experimental constrictions (*n*=326 edges from 21 constrictions). Bin width, 1.5 min. Plotted points are mean±s.d.

levels (Kitayama et al., 1997), whereas aberrant septum growth with disjoint patches of septal material has been observed in temperature-sensitive mutants of the contractile ring proteins profilin Cdc3, myosin light chain Cdc4, and tropomyosin Cdc8 (Streiblova et al., 1984). Mutations in Bgs proteins can also influence the ring. For instance, in cells with reduced levels of Bgs4, constriction of the contractile ring appears to be faster than septum ingression (Muñoz et al., 2013).

Here, we present experimental and theoretical evidence that the contractile ring tension regulates septum shape during cytokinesis by locally controlling growth rates. We measured ingrowing septum edges in live cells and quantified their deviations from circularity by the edge roughness, borrowing a classic definition from materials physics (Lapujoulade, 1994). The edges were inconsistent with independent Bgs-mediated growth processes, which would produce scale-independent roughness that always increased over time. Instead, roughness increased with length scale according to a power law, i.e. the difference between the radial coordinates of any pair of points on the edge was greater for points separated by a greater distance along the septum edge. Further, the roughness of the edges first peaked and then decayed over time. In cells that lacked intact actomyosin rings, septa constricted but had much greater roughness. To explain these findings we postulate that Bgs-mediated synthesis of septum is mechanosensitive, and that the contractile ring communicates mechanically with the machinery of septum synthesis. A mathematical model shows that this mechanism generates smooth, circular septum edges with a roughness that peaks over time and has power-law dependence on length scale that is close to the one observed. Our results suggest that cytokinetic ring tension does not set the rate of constriction, but regulates circularity of the septum and its defect-free closure through its effect on mechanosensitive Bgs-mediated growth processes.

RESULTS

Ingressing septum edges during fission yeast septation have a roughness of ~5% of the ring radius that decreases in time

We sought to quantify the deviation from circularity of septum edges during cytokinesis in *S. pombe*, and to test whether growth at the septum edge is spatially coordinated such that the edge is regulated to become smooth and circular. We extracted edges from experimental images and quantified their roughness, the root mean square (rms) fluctuation in height, a common measure of irregularity (Lapujoulade, 1994).

We used confocal microscopy to image cells expressing GFP-Bgs4 or RFP-Bgs4, which localize to the surface of the septum, and myosin-II light chain Rlc1-GFP or the F-BAR-domain-containing protein Cdc15-Tomato, which localize to the contractile ring (Cortés et al., 2005; Le Goff et al., 2000; Roberts-Galbraith et al., 2009) (Fig. 1B). During constriction Bgs4 was distributed on the entire septum surface up to the location of the contractile ring, showing that the ring followed the inner septum edge and suggesting that Bgs4 reliably marked the edge. We traced septum edges using the Canny edge detection method based on intensity gradients (Fig. 1B, supplementary material Fig. S2A, and Materials and Methods). The mean radius of septum edges decreased linearly in time with a mean constriction rate 80±10 nm/min (mean±s.d., *n*=21 constrictions) (Fig. 1C).

For an edge grown by independent random growth processes the roughness always increases in time (Lesne and Laguës, 2012). To test septum edges for this feature we fit best circles to measured edges and determined the deviations from circularity $h(s)$ and, hence, the roughness $w_{sept}=\langle(\delta h)^2\rangle^{1/2}$ (Fig. 1B,D-F and Materials and Methods). Here, δh denotes the deviation from the mean and the average is over all points on the edge. The roughness of septum edges decreased in time, in some cases showing an early increase before peaking and decreasing (Fig. 1F, supplementary material Fig. S1A). The mean time averaged roughness was 31±9 nm (mean±s.d.) over *n*=326 septum edges from 21 cells. Throughout, a 'septum edge' refers to a septum at one instant in time, and the statistics we present are averaged over many edges, i.e. we report averages over time and over different cells. The mean roughness is a small fraction 5.0±1.8% of the septum radius, and the roughness does not show the steady increase in time characteristic of uncorrelated growth processes.

The roughness of septum edges increases with length scale and follows a power law

If septum edges are grown by statistically independent septum synthesis processes around the edge, at any instant the roughness would have a constant value that is independent of length scale, whereas – if the septum shape is regulated – growth rates at different locations would be correlated. A hallmark of spatially correlated growth is scale-dependent roughness: the longer the section of the edge, the bigger the fluctuations and the roughness within that section (Lesne and Laguës, 2012).

To test for growth correlations, we calculated the mean roughness on the scale x, $w(x)=\langle(\delta h)^2\rangle_x^{1/2}$, where the average is over all points in a given section of the septum edge of length x, and then over all such regions (Fig. 1E, and Materials and Methods). The roughness of edges increased with length scale up to a saturation scale x_{sat} (Fig. 2A). For practical reasons, we define x_{sat} as the scale where roughness attains 80% of its maximum value w_{sept}. The x_{sat} versus time curve, averaged over all edges, increased, peaked after ~5 min and, thereafter, decreased (Fig. 2B). Values of roughness and x_{sat} varied considerably from cell to cell (supplementary material Fig. S1A,B), and for many individual cells we did not record a peak in x_{sat}, possibly because imaging commenced after the peak occurred. Averaged over all edges, roughness followed a power law $w\sim x^\alpha$ for $x<x_{sat}$, with best-fit exponent $\alpha=0.47\pm0.03$ (95% confidence interval, $n=326$ septum edges from 21 cells) (Fig. 2C). Thus, septum edges are grown by spatially coordinated processes and have a characteristic roughness exponent.

The values of roughness we report, $\lesssim$40-50 nm, are less than the pixel size (~65 nm) of our images and the estimated confocal microscopy point spread function (psf) width (~200 nm). To test our method, we generated artificial septum edges with a roughness exponent $\alpha=0.5$ and variable roughness (supplementary material Fig. S2B-I). We mimicked confocal imaging of these edges with a pixel size of 65 nm and a psf width of 200 nm; we applied our edge detection algorithm to these 'images', and we measured roughness w_{sept} and exponent α of these detected edges. For test data edges with an actual roughness of ~30 nm – typical of the values we report in this study – our measurement procedure produced a similar roughness and an exponent of ~0.37. This test suggests that our method reproduces actual roughness to within ~20% of the actual value but somewhat underestimates the roughness exponent (see supplementary material Fig. S2).

Mathematical model of septum growth regulated by ring tension

Because the contractile ring is attached to the plasma membrane adjacent to the septum, the ring tension might mechanically influence the septum and the processes that synthesize it. The ring might have direct mechanical interactions with Bgs complexes because Bgs1p is an integral membrane protein (Liu et al., 2002). To examine whether such effects can explain the highly correlated growth we observed, we developed a model of the stochastic centripetal growth of the inner septum edge that closes down the septum, assuming septum synthesis is mechanosensitive. Here, we outline the main features of the model (for further details, see Materials and Methods).

The radius of the inner septum edge is defined to be $r(s,t)=R(t)+h(s,t)$ at location s on the edge at time t (Fig. 1B). Here, $R(t)$ is the mean radius and $h(s,t)$ the deviation from circularity at s (Fig. 1B,D,E). We assume that the inward growth velocity $v_{sept}(s,t)\equiv-\partial r/\partial t$, due to Bgs complex-mediated synthesis of
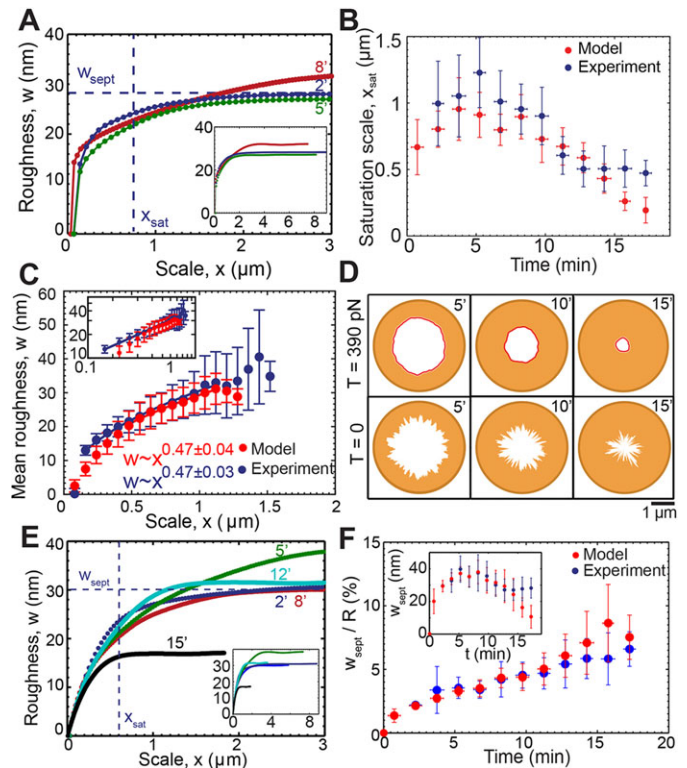

Fig. 2. Roughness of septum edges is length scale dependent and follows a power law reproduced by a model of septum growth regulated by ring tension. Supplementary material Table S1 lists the model parameters. (A) Roughness w versus length scale x for the septum edges of Fig. 1B at the indicated times. Dashed lines indicate w_{sept} and x_{sat} at time point 2 min. Inset shows full roughness profiles. (B) Roughness saturation length x_{sat} versus time for experimental constrictions of Fig. 1F (blue) and simulated constrictions (red); simulation: $n=428$ edges from 30 constrictions. Points are mean±s.d. Bin width, 1.5 min. (C) Mean roughness w versus length scale x for the experimental and simulated constrictions shown in B. For each x, the mean is over all constrictions, for which $x<x_{sat}$ and over all times. The exponent of the best-fit power law to simulated data is 0.47±0.04 (95% confidence interval) for 0.48 µm$\leq x\leq$1.12 µm . Error bars denote s.d. Inset shows plot of log mean roughness versus log length scale x. (D) Typical simulated septum edges at indicated times (min) after the onset of constriction at two tensions. (Top row) T=390 pN as measured in protoplasts. (Bottom row) T=0. (E) Roughness w versus scale x for simulated constrictions as shown in D, at T=390 pN. Dashed lines indicate maximum roughness w_{sept} and roughness saturation scale x_{sat} after 2 min. Inset shows complete roughness profiles for the same edges. (F) Ratio of septum roughness to mean septum radius versus time for simulated and experimental constrictions and times of B. Inset shows septum roughness versus time for same data. Bin width, 1.5 min. Points are mean±s.d.

septum, depends on the radial force per unit length γ, which is exerted on the septum at that location by the contractile ring,

$$v_{sept}(s,t) = v_{sept}^0\left(1 + \frac{\gamma(s,t)}{\gamma^*}\right) + \eta_{fluc}(s,t). \qquad (1)$$

Here, v_{sept}^0 is the intrinsic growth velocity of the septum edge. The force is communicated to the septum synthesis apparatus and, thereby, accelerates growth by the factor γ/γ^*, where γ^* is a response threshold for the molecular machinery. The crucial term η_{fluc} represents fluctuations of the growth rate about the mean whose strength λ sets the magnitude of the edge roughness. This term describes independently operating growth machines around the septum $\langle\eta_{fluc}(s,t)\eta_{fluc}(s',t')\rangle=\lambda\,\delta(s-s')\delta(t-t')$. It is the force term in Eqn 1 that will introduce growth correlations and shape regulation.

The centripetal force exerted by the contractile ring of tension T is given by Laplace's law $\gamma = T(1/R - \partial^2 h/\partial s^2)$. Crucially, this force depends on the local curvature $\partial^2 h/\partial s^2$ of the ring, which is equal to the septum curvature, because the shape of the ring is the same as the shape of the septum edge, albeit separated from it by a few nanometers. As seen using Eqn 1, growth will be faster where the edge has large and negative curvature (troughs), and suppressed where curvature is positive (bumps). This hypothesis is consistent with reported correlations between local septum curvature and growth rate in deformed yeast cells (Zhou et al., 2015). Overall, we expect that through this mechanism ring tension will tend to restore circularity.

Using this expression for the force in Eqn 1 yields the basic equations for septum growth (see Materials and Methods):

$$\frac{\partial h}{\partial t} = D\frac{\partial^2 h}{\partial s^2} + \eta_{\text{fluc}}, \qquad -\frac{dR}{dt} = v_{\text{sept}}^0 + \frac{D}{R}, \qquad D = \frac{v_{\text{sept}}^0 T}{\gamma^*} . \quad (2)$$

The first equation tells us that septum edge fluctuations h obey the diffusion equation plus a noisy source term η_{fluc}, with an effective diffusivity D that is proportional to the ring tension T. Thus, random growth excites septum edge fluctuations but ring tension acts to smooth out these irregularities much like molecular diffusion smoothens density inhomogeneities in other contexts. These dynamics for h are similar to those in the classic Edwards–Wilkinson equation that describes stochastic interfacial growth processes (Edwards and Wilkinson, 1982), with the complication that, here, the growing surface is curved and continuously shortening, $0 < s < 2\pi R(t)$. The second result of Eqn 2 states that the mean constriction rate is increased due to the tension of the ring by an amount D/R, an increasingly strong effect as the ring shortens. We developed a computer simulation to implement this model on an initially circular lattice of points representing the septum edge that was evolved according to Eqn 2 (see Materials and Methods).

Simulations close septa properly, and reproduce experimental constriction curves and roughness profiles

We simulated our model using the parameter values provided in supplementary material Table S1. Simulated septum edges regulated by rings with normal tension remained close to circular and achieved proper closure, constricting down almost to a point (Fig. 2D), whereas unregulated septum growth produced rough irregular edges that closed improperly (Fig. 2D). By fitting the mean initial slopes of simulated constriction curves to the experiment (mean septum radius R versus time), we obtained the intrinsic septum growth rate $v_{\text{sept}}^0 = 72 \pm 12$ nm/min. With best-fit parameters (see below) constriction curves showed little downward curvature – in agreement with the experiment – with a mean constriction rate of 86±3 nm/min (supplementary material Fig. S1C) (n=428 edges from 30 constrictions) that was only ~20% greater than the intrinsic septum growth rate and consistent with the experimental value measured here (80±10 nm/min) and previously reported values (Pelham and Chang, 2002).

For each simulated constriction we calculated the roughness profile $w(x)$ of the septum edge at different times as the edge constricted over ~20 min. As seen experimentally (Fig. 2A), at each time the roughness increased with length scale up to a plateau value w_{sept} at the roughness saturation length scale x_{sat} (Fig. 2E, supplementary material Fig. S1D). We used the saturation scale to extract the diffusivity parameter D: we fit the model-predicted time dependence of the saturation scale to experiment, averaged over all constrictions (n=21 experimental and n=30 simulated

constrictions), using D as a fitting parameter (supplementary material Fig. S1E). With the best-fit value D=180±130 nm^2/s (±95% confidence interval; supplementary material Fig. S1E), the predicted and measured curves were in close agreement (Fig. 2B).

The model predicts a roughness exponent of ~0.5 – close to the experimental value

Our experiments showed a septum edge roughness exponent α=0.47 (Fig. 2C). Given that our model is close to the Edwards–Wilkinson model of randomly growing interfaces, for which $w(x) \sim \sqrt{\lambda x/D}$ has an exponent α=0.5 (Edwards and Wilkinson, 1982), we anticipated that simulated septa would have a roughness exponent close to the experimental value. To test this, we averaged simulated roughness profiles $w(x)$ over time and over n=30 distinct constriction runs, and fit the mean profile to the averaged experimental profile with the previously determined value for D, and using the growth fluctuation strength λ as a fitting parameter that sets the amplitude of the roughness (Fig. 2C). To focus on the power law regime, the averaging procedure was confined to the increasing part of each profile, in the window of length scales that are larger than the growth correlation length of the Bgs complex and the experimental pixel size, but less than the saturation scale x_{sat} (see Materials and Methods). This yielded λ=4100±2100 nm^3/s (±95% confidence interval, supplementary material Fig. S1F).

With these parameter values, the averaged simulated roughness profile was well-described by a power law $w \sim x^{\alpha}$ with a best-fit exponent α=0.47±0.04 (±95% confidence interval, n=428 edges from 30 constrictions), matching the experimental value α=0.47±0.03 (Fig. 2C). Thus, our experimental results are consistent with a ring-tension-mediated and curvature-sensitive mechanism that regulates local septum synthesis rates.

Consistent with experiments, simulated septum edges are nearly circular, presenting low roughness values

Consistent with the time dependence measured in live cells, the total roughness w_{sept} of simulated edges increased, peaked and then decreased over time (Fig. 2F, supplementary material Fig. S1G). The decrease at late times occurs because the nominal value of x_{sat} then exceeds the septum length, so growth at all points is correlated and total roughness then increases with septum length. The mean time averaged simulated roughness was w_{sept}=30±10 nm (mean± s.d.), a small fraction 4.3±2.4% of the ring radius (mean±s.d.) and consistent with the experimental value of 31±9 nm. The mean aspect ratio of simulated septum edges was 1.09±0.10 (mean±s.d.), close to the value of 1 for a circle and close to the experimental ratio of 1.09±0.05 (supplementary material Fig. S3A). During constriction, ring tension corrected deviations from circularity by appropriately adjusting growth rates (supplementary material Fig. S3B-F).

Contractile ring tension is sufficient to suppress septum roughness but insufficient to substantially affect constriction rates

We used the model to vary the tension over a broad interval $0 < T < 1000$ pN, surrounding the value $T \sim 400$ pN reported in live cells (Stachowiak et al., 2014), for which septum roughness peaked and then decayed over time, and the aspect ratio remained close to unity (Fig. 2D, supplementary material Figs S3G and S4A). By contrast, septa closed improperly in the absence of ring tension with aspect ratios far from unity and increasing septum roughness with time. Increasing tension from zero to the physiological value decreased septum roughness by a factor of ~4 (from 116±46 nm to

30±10 nm), but further increase to 1000 pN had little effect (Fig. 3A). As expected, higher tensions produced constriction curves $R(t)$ with greater curvature (see Eqn 2) that significantly exceeded the experimental value at the highest tension (Fig. 3B). Thus, the contractile ring tension in cells is just high enough to substantially suppress the roughness that uncorrelated septum growth would generate, yet insufficient to substantially increase the constriction rate.

Septum synthesis has a mechanosensitivity of ~0.1 pN^{-1} per Bgs complex

According to our model the suppression of septum roughness by ring tension is quantified by the diffusivity $D=v_{sept}^0 T/\gamma^*$, which depends on the ring tension T, the intrinsic septum growth rate v_{sept}^0 and the parameter γ^*, the mechanical force per unit length that increases the synthesis rate of the septum-growing apparatus twofold. By using values for D and v_{sept}^0 from fitting the model to experiment and the measured tension of the *S. pombe* ring (supplementary material Table S1) gives $\gamma^*=2.61\pm1.89$ pN/nm, which is approximately five times the typical force per unit length exerted by the ring, T/R. This reflects the fact that ring tension has little effect on the mean constriction rate, while being sufficient to significantly affect high-curvature troughs or bumps.

If one were to assume that the leading septum edge is grown by Bgs1p alone, this would give a density of active Bgs1p at the septum edge $\rho_{bgs} \sim 0.4$ nm^{-1} after estimating for simplicity that 50% of the ~8000 Bgs1p molecules (Arasada and Pollard, 2014) at the cleavage furrow localize to the edge and are active. Hence, the mechanosensitivity for the septum synthesis apparatus on a per Bgs1p basis is $\mu^*=\rho_{bgs}/\gamma^*=0.15\pm0.10$ pN^{-1}. This represents the relative synthesis rate increase per unit force.

Ring disassembly or mutations in contractile ring components yield septa with increased roughness, shape irregularities and growth rate inhomogeneities

Because our results suggest that ring tension controls local septum synthesis, we next examined the effects the disruption of the ring has by mutating three different contractile ring proteins and by treatment with Latrunculin A (LatA) to depolymerize actin filaments. LatA treatment and disablement of formin Cdc12 increased the roughness (Fig. 4C), the roughness exponents (Fig. 4D, supplementary material Fig. S4C) and the aspect ratios (supplementary material Fig. S4A) of the septum more than depletion of F-BAR Cdc15p or deletion of the IQ motifs from the IQGAP protein Rng2p (supplementary material Fig. S4B).

LatA treatment

We added 200 µM of the actin-monomer-sequestering agent LatA, sufficient to disassemble the F-actin ring and abolish actomyosin

activity within 1 min of treatment, to cells 2–5 min before imaging (Pelham and Chang, 2002). LatA-treatment fragmented the contractile ring and, over time, the septum holes moved off-center, becoming more irregular and increasingly slit-shaped (Fig. 4A), as noted previously (Zhou et al., 2015). The roughness of 149±73 nm, the roughness exponent of 1.02±0.10 and the aspect ratio of 1.77±0.69 were all much larger than those from wild-type (Fig. 4C,D, supplementary material Fig. S4A).

Temperature-sensitive Cdc12 mutant

Contractile rings disassemble within ~4 min after shifting the temperature-sensitive formin mutant *cdc12-112* to the restrictive temperature (Zhou et al., 2015), presumably due to loss of actin filaments. Over time at the restrictive temperature, the septum edges became rougher and more elongated (Fig. 4A,B). Given the absence of F-actin, actomyosin activity is, presumably, abolished in these cells. The roughness of 73±42 nm, the roughness exponent of 0.88±0.07 and the aspect ratio of 1.25±0.10 were above those of the wild-type (Fig. 4C,D, supplementary material Fig. S4A).

Rng2 mutant

We imaged *rng2Δ* deletion mutant cells complemented with Rng2pΔIQ, a construct of the ring component IQGAP Rng2p that lacks IQ motifs ('Rng2pΔIQ') using a confocal microscope setup with a somewhat larger pixel size of 83 nm. The septa in dividing Rng2pΔIQ cells moved off center but remained almost circular and closed properly (Fig. 4A). The roughness of 43±14 nm, the roughness exponent of 0.45±0.03 and the aspect ratio of 1.09±0.07 of the septa were close to those of wild-type (Fig. 4C,D, supplementary material Fig. S4A).

Cdc15 depletion

We grew *41xnmt1cdc15* cells under conditions that reduce the amount of the F-BAR protein Cdc15p to 15% of wild-type levels. This reduces the initial rate of septum growth owing to slow delivery of Bgs1p to the division site (Arasada and Pollard, 2014). Septa in dividing *41xnmt1cdc15* cells remained almost circular and closed properly (Fig. 4A), with a roughness of 47±15 nm, a roughness exponent of 0.45±0.05 and an aspect ratio of 1.11±0.06, which are similar to wild-type cells (Fig. 4C,D, supplementary material Fig. S4A).

The results of these experiments are consistent with the ring serving to control septum roughness and shape. To model septation without a functional ring, we used our simulations with zero ring tension, which produced a roughness similar to that in the experiments (116±46 nm, Fig. 4C) but with almost no dependence on length scale, as expected of independently operating septum synthesis processes (supplementary material Fig. S4D).
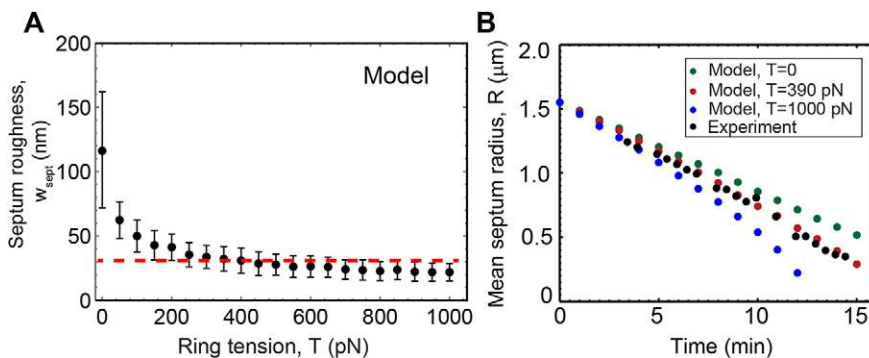

Fig. 3. Cytokinetic ring tension is sufficient to curtail septum roughness without significantly affecting constriction rate. (A) Mean roughness of simulated septa versus tension, after fixing other parameters as described in supplementary material Table S1. Each point is the average over *n*=360 edges from 30 constrictions. Error bars indicate ±s.d.; the dashed line indicates the experimental mean septum roughness from constrictions of Fig. 2B, averaged over constrictions and times. (B) Simulated mean septum radii versus time for three values of ring tension, compared to a typical experimental constriction.
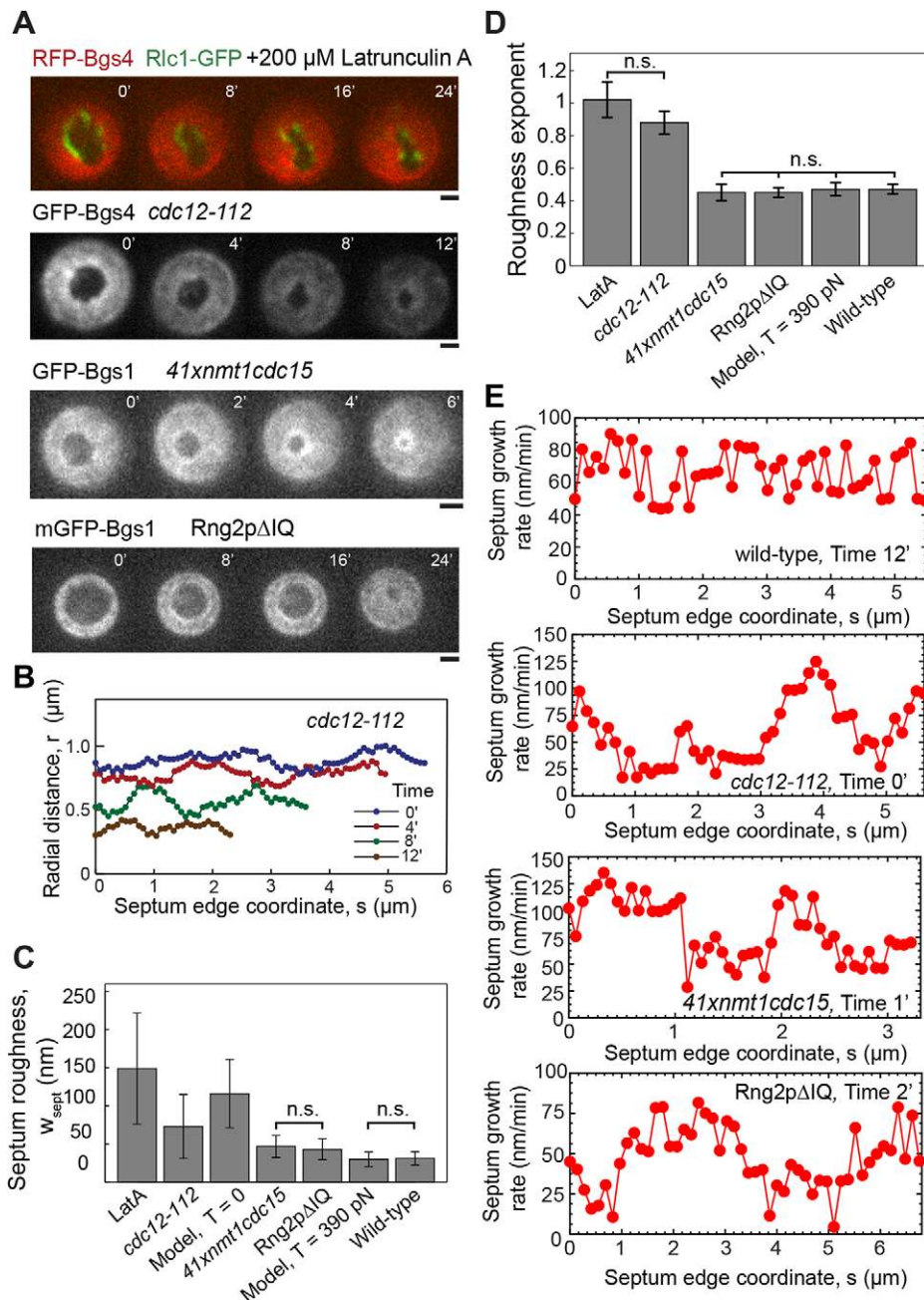
Fig. 4. Septa with abnormal roughness, deviations from circularity and inhomogeneous growth rates in cells treated with LatA or with mutations of contractile ring proteins. n.s. denotes that there were no statistically significant differences within the indicated group (*P*>0.05). (A) Confocal fluorescence micrographs of division planes during constriction in a wild-type yeast cell expressing RFP-Bgs4 and Rlc1-GFP and treated with 200 μM LatA, a *cdc12-112* cell expressing GFP-Bgs4 and Rlc1-Tomato at the restrictive temperature, a *41xnmt1cdc15* cell expressing GFP-Bgs1p, Rlc1p-tdTomato and Sad1p-GFP, and a *rng2Δ* cell expressing mEGFP-Bgs1p, Sad1-RFP and complemented with Rng2pΔIQ. Times in minutes after the first frame. Scale bars: 1 μm. (B) Radial distance profiles of the septum edges in the *cdc12-112* cell of A at four times. (C) Comparison of mean septum edge roughness in wild-type cells (Fig. 2B), the cases shown in A, and simulations with and without tension. Roughness was calculated from constrictions shown in Figs 2B, 3A, supplementary material Fig. S4A. Error bars indicate ±s.d. (D) Comparison of exponents of septum edge roughness for the same cases as shown in C, except for zero tension simulations. Exponents from Fig. 2C, supplementary material Fig. S4B,C. Error bars denote ±95% confidence intervals. (E) Septum growth rate versus edge coordinate s for the wild-type, *cdc12-112*, *41xnmt1cdc15* and Rng2pΔIQ cells as shown in Figs 1B and 4A. Growth rate is the mean value over an interval of 2 min (wild-type, *41xnmt1cdc15*) or 3 min (*cdc12-112*, Rng2pΔIQ). Growth rates of *cdc12-112*, *41xnmt1cdc15* and Rng2pΔIQ cells show large systematic spatial fluctuations, unlike those of wild-type cells.

We also observed that the edges of the septa in all three mutant strains and LatA-treated cells underwent large systematic variations in growth rates over scales of ~1–2 μm around the septum edge, about one quarter of the edge length (Fig. 4E). This behavior was manifested as high-amplitude anticorrelations in the velocity correlation function on a similar scale (supplementary material Fig. S4E,F). By contrast, in wild-type cells the velocity variations are less and correlations are absent at scales of ≳0.5 μm (Fig. 4E, supplementary material Fig. S4E). We also note occasional edge segments of lengths ≲0.5 μm that exhibited an almost uniform growth rate in *cdc12-112*, wild-type and *41xnmt1cdc15* cells.

The extended spatial variations we observe might reflect an inhomogeneous distribution of Bgs complexes related to the absence of or damage to the contractile ring, beyond the scope of our model. Indeed, previous studies showed altered Bgs localization in *41xnmt1cdc15* and Rng2pΔIQ cells. In *41xnmt1cdc15* cells the

ring slid along the long axis of the cell until ~2000 Bgs1p molecules accumulated adjacent to the ring, and the amount of Bgs1p at the ring at the onset of constriction was ~30% lower than in wild type (Arasada and Pollard, 2014). Rng2pΔIQ cells have reduced levels of the SIN kinase Sid2p at the division plane and an altered Bgs1p distribution compared with wild-type cells (Tebbs and Pollard, 2013). In LatA-treated cells, the Bgs1p distribution is anisotropic and, interestingly, spatial variations in growth rate correlate with Bgs and Rlc1p localization (Zhou et al., 2015).

DISCUSSION
Stochastic growth leads to rough interfaces

Surface growth phenomena, such as crystallization and corrosion, abound in nature (Hermann et al., 1995; Stegemann et al., 2004). Intrinsic molecular stochasticity can produce irregularities in the growing interfaces, commonly described by the roughness, the rms

fluctuation in height (Lapujoulade, 1994). Roughness is caused by spatial variations in growth rates that produce height differences, and is typically moderated by lateral diffusion or other smoothing effects that tend to equalize these heights. The net result is a roughness $w(x)$ that depends on length scale x: nearby points (small x) have similar heights owing to diffusive smoothing, whereas more separated locations are less affected by diffusion and height differences are greater. The classic Edwards–Wilkinson and Kardar–Parisi–Zhang models of interfacial growth in the presence of diffusive smoothing predict a power law dependence $w(x) \sim x^{\alpha}$ with a roughness exponent $\alpha=0.5$ (Edwards and Wilkinson, 1982; Kardar et al., 1986).

Septum growth is spatially coordinated during septation in *S. pombe*

Stochastic growth also occurs in cells; it occurs in septation during cytokinesis in fungi and bacteria when cell wall synthases grow the division septum (Balasubramanian et al., 2012; Pollard and Wu, 2010), in the assembly of microtubules or actin filaments in the cytoskeleton (Desai and Mitchison, 1997; Vavylonis et al., 2005) or in polymerase-mediated DNA synthesis from nucleotides (Geertsema et al., 2014). In such cases, molecular randomness leads to shape or length fluctuations in the assembled structures.

Here, we studied septation mediated by glucan synthases that reside in the plasma membrane in fission yeast. Growing septum edges were almost circular, with a scale-dependent roughness that was small (Fig. 2C). Were growth spatially uncoordinated, a high roughness would be expected down to the smallest scales, and would, presumably, lead to improper septum closure. Given that septa close properly, and given the scale-dependent edge statistics, we conclude that septum growth is spatially coordinated.

The contractile ring regulates septum roughness and directs proper septum closure

What mechanism achieves this coordination? To equalize growth rates around the septum with sufficient fidelity to maintain an almost perfectly circular septum edge would be demanding of a mechanism based on long-range biochemical communication between edge locations that are microns apart. We proposed that septum growth rates are spatially coordinated by a robust, short-ranged mechanism that prevents edge irregularity that would otherwise result (Fig. 5A), based on the hypothesis that the contractile ring is mechanically coupled to the septum synthesis process.

The molecular mechanism is unknown, but a conceptually simple possibility is a direct interaction with the integral membrane Bgs complexes (Fig. 5B). Other possibilities include stretching of the septum material to locally enhance synthesis rates.

A mathematical model showed that forces due to ring tension T then suppress roughness by adjusting growth rates to an extent that depends on the local septum curvature (Fig. 5C), analogously to diffusive smoothing. The smoothing mechanism is quantified by a diffusivity parameter $D=v_{\text{sept}}^{0}T/\gamma^{*}$ (Eqn 2). The predicted roughness exponent $\alpha \sim 0.47$ was close to the Edwards–Wilkinson model and experimental values (Fig. 2C). Simulated septa remained circular and closed without defects (Fig. 2D, supplementary material Fig. S3A), and the roughness saturated in time as seen experimentally (Fig. 2F). These results support the hypothesis that the ring maintains circularity of the septum and its defect-free closure by regulating mechanosensitive septum synthesizing apparatus.

Mechanosensitivity of septum synthesis machinery enables shape regulation

We defined the mechanosensitivity as the rate of increase of septum synthesis rate per applied force, relative to the intrinsic rate without force. From the best-fit value of the diffusivity parameter $D=180$ nm^{2}s^{-1}, we found a mechanosensitivity $\mu^* \sim 0.15$ pN^{-1} on a per-Bgs-complex basis. If we assume that Bgs complexes are themselves directly affected (Fig. 5B), this would imply a ~ 0.15 pN^{-1} sensitivity of the synthase, which is considerably higher than that of another molecular polymerization complex – RNA polymerase II of *S. cerevisiae* – for which we estimate $\mu^* \sim 0.01$ pN^{-1} at saturating NTP conditions (Larson et al., 2012). By contrast, the sensitivities estimated from constructs of the actin polymerization regulators formin Bni1p and mDia1, which contain the catalytic FH1-FH2 domains, are somewhat greater, $\mu^* \sim 1$ pN^{-1} and $\mu^* \sim 0.4$–0.5 pN^{-1}, respectively (Courtemanche et al., 2013; Jégou et al., 2013).

The role of the cytokinetic contractile ring

Our study suggests that, in fission yeast, the tension of the contractile ring controls septum shape but has very little influence on the rate of constriction. A tension of ~ 400 pN was measured in the contractile ring in fission yeast protoplasts (Stachowiak et al., 2014), and the ring is commonly thought to drive cell division and set the constriction rate. However, such tensions are unlikely to directly mechanically affect the septum beyond negligible strains ($\sim 0.01\%$), given the cell wall modulus of ~ 30 MPa (Minc et al., 2009) and the ring width of $w_{\text{ring}} \sim 0.1$ μm (Kanbe et al., 1989). Ring bending rigidity is expected to exert even weaker forces on the septum (Stachowiak et al., 2014). Thus, inward growth of the rigid septum limits the rate of constriction. Moreover, septa can complete constriction without a ring (Proctor et al., 2012) and, in yeast protoplasts, rings constrict at variable speeds depending on the local slope of the plasma membrane, suggesting the constriction rate is not an intrinsic property of the ring (Stachowiak et al., 2014).

The possibility remains that the ring tension indirectly affect constriction rates by boosting the rate of septum synthesis. Our analysis suggests this is not so; the tension is sufficient to curtail roughness but the constriction rate is set by the rate at which septum is synthesized, little affected by ring tension (Figs 2F and 3A,B). This originates in the incoherent nature of growth fluctuations that tend to self-cancel: during constriction the net septum area produced by fluctuations $(\lambda R_0 \tau_{\text{constrict}})^{\frac{1}{2}} \sim 0.06$ μm^2 is much less than the total septum area grown $\pi R_0^2 \sim 7.5$ μm^2, where R_0 is the initial radius. Thus, fluctuations are relatively easily influenced. We found that the value of ring tension in cells lies within a broad window in which roughness is affected but not the mean constriction rate (Fig. 3A,B).

If the ring tension has only a small effect on the rate of septation, why are constriction rates lower in Rng2p mutants that lack IQ motifs, in temperature-sensitive *myo2* mutant *myo2-E1* cells and in *cdc12-112* cells at the restrictive temperature (Proctor et al., 2012; Tebbs and Pollard, 2013)? This might be because mutations in ring components affect septation in many ways, independently of ring tension. Indeed, Rng2p mutations resulted in fewer molecules of Sid2p kinase (a septation initiation network kinase) in rings (Sparks et al., 1999; Tebbs and Pollard, 2013), and altered the spatial distribution of Bgs1p in the cleavage furrow (Tebbs and Pollard, 2013).

The most direct evidence that the ring tension T does not accelerate septation comes from measurements in wild-type fission yeast uncomplicated by systemic effects of mutations, together with
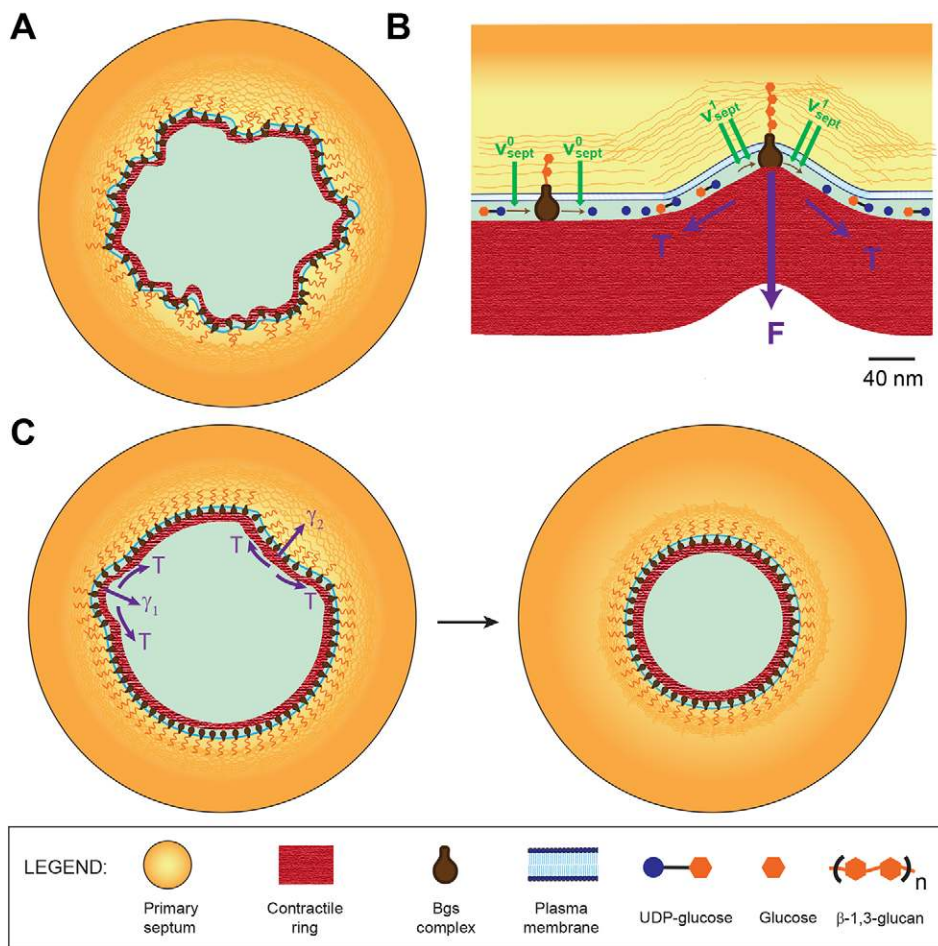
Fig. 5. Model of septum shape regulation through cytokinetic ring tension. UDP-glucose, glucose and β-glucan are not to scale. (A) If septum synthesis rates were statistically independent around the septum, intrinsic fluctuations in local growth rates would produce irregular septum edges with high roughness. (B) Hypothetical mechanism for mechanosensitivity of septum synthesis based on direct mechanical coupling between the contractile ring (at tension T) and β-glucan synthase complexes in the plasma membrane. At flat locations septum is synthesized at the base rate (v_{sept}^0, left). Where curvature is high, the ring exerts force F on Bgs complexes, increasing the rates of polymerization and septum synthesis ($v_{sept}^1 > v_{sept}^0$, right). (C) In the presence of the tense ring, the mechanism described in B smoothes edges and maintains circularity. At a bump (negative curvature, right) the outward force per unit length γ_2 suppresses the rate of Bgs synthesis, whereas at a trough (positive curvature, left) the inward force per unit length γ_1 increases the rate of synthesis. The net effect is to reverse such deviations and restore circularity.

Laplace's law, which dictates that the ring exerts an inward force per unit length T/R. If the mean septum growth rate were influenced by this force, constriction would accelerate dramatically as the ring radius R becomes small. On the contrary, experimental constriction rates are almost constant (Pelham and Chang, 2002). Experiment and modeling suggest this is not owing to decreasing ring tension as constriction proceeds, because the concentration of myosin II in the ring increases (Wu and Pollard, 2005) and the predicted tension increases accordingly (Stachowiak et al., 2014). Thus, in the picture emerging from our study, once the ring and septum synthesis apparatus are in place, it is septum synthesis that sets the rate of constriction whereas the ring coordinates growth spatially to ensure proper closure.

MATERIALS AND METHODS
Yeast strains and media
Standard methods were used for genetic manipulation and media. Strains are listed in supplementary material Table S2. Wild-type, *cdc12-112*, and LatA-treated cells were incubated in PDMS chambers in YE medium and imaged in the lab of Fred Chang (Columbia University). *cdc12-112* cells were imaged 5–10 min after imposition of 36°C. Wild-type and LatA-treated cells were imaged at 25°C. Experiments using LatA used latrunculin at a concentration of 200 µM, obtained by adding 20 mM LatA stock to yeast cells in DMSO. LatA was added to cells 2–5 min prior to imaging. *41xnmt1cdc15* and Rng2pΔIQ cells were incubated in PDMS chambers at 25°C in EMM5S medium and imaged in the lab of Thomas D. Pollard. Three *z*-slices 0.4 µm apart were acquired to cover the entire septum for wild-type, *cdc12-112* and LatA-treated cells. Six *z*-slices 1.8 µm apart were used for *41xnmt1cdc15* and Rng2pΔIQ cells. Images used for quantitative analysis were sum-intensity projections of these slices. Some images used in

this study were provided by Zhou Zhou and Fred Chang, Columbia University. PDMS chambers used by them to orient cells vertically were developed by Jun He, Emilia Laura Munteanu, Zhou Zhou, Mark Bathe and Fred Chang. The development and use of these chambers are described elsewhere (Zhou et al., 2015). Imaging of *41xnmt1cdc15* and Rng2pΔIQ was performed using PDMS chambers created at Yale School of Engineering and Applied Sciences, using soft lithography techniques described in Wang and Tran (2014). Procedures for growing and preparing *41xnmt1cdc15* and Rng2pΔIQ cells for imaging are identical to those used in Tebbs and Pollard (2013) and Arasada and Pollard (2014), except cells were imaged in PDMS chambers.

Microscopy and image analysis
Wild-type, *cdc12-112*, LatA: Images were acquired using a spinning-disc confocal (CSU10; Yokagawa) on an inverted microscope (Nikon Eclipse Ti) with a EM-CCD camera (Hamamatsu) and 100×1.4 NA objective with a 1.5× magnifier. The resulting images have pixel size 65.3 nm and were acquired at intervals of 5 s, 30 s, 1 min and 2 min. Temperature was controlled using an objective heater (Bioptechs). Image acquisition was performed using Micromanager 1.4 (Edelstein et al., 2010). *41xnmt1cdc15*, Rng2pΔIQ: Microscope set-up details as in Tebbs and Pollard (2013).

The MATLAB implementation of the Canny edge detection method was applied separately to every frame of every experimental movie, with low and high thresholds of edge detection equal to 0.1 and 0.6, and a standard deviation of σ=2.5 pixels for the Gaussian smoothing procedure, which is the first step of the Canny method (Canny, 1986). These parameters were chosen to maximize the number of successfully detected septum edges. A continuous closed boundary at the inner edge of the fluorescently tagged Bgs4 signal is considered as a successfully detected septum edge.

We obtained best-fit circles and ellipses to septum edges using methods described in Umbach and Jones (2003), to calculate mean radius and aspect ratio. To determine initial septum radius R_0, we used circles fit to hand-drawn septum edges because edge detection failed at onset of septation. All other frames in which edges could not be successfully detected were excluded from further analysis.

Calculation of septum edge roughness

The irregularity of an interface can be quantified by its roughness, the rms fluctuation in the height of the interface measured perpendicular to a reference shape. This measure is widely used in materials science (Lapujoulade, 1994). We measured the 'height' of the septum as the deviation from circularity, by using best-fit circles to each septum edge as the reference shape. The height is $h(s)=r(s)-R$, where R is the radius of the best-fit circle and $r(s)$ is the radial coordinate of the septum edge at coordinate s, where $0 \leq s \leq 2\pi R$. Here, the coordinate s is the distance around the best-fit circle. A discrete set of s values was used, corresponding to individual pixels.

For a given septum edge, roughness over the length scale x, $w(x)$, is defined as:

$$w(x)=\langle(\delta h)^2\rangle_x^{\frac{1}{2}} = \left\langle\left(\frac{1}{x}\int_{s=s_0}^{s_0+x}(r(s)-R)^2\,ds\right)\right\rangle^{\frac{1}{2}}, \quad (3)$$

where angular brackets denote averaging over all parts of the septum edge of length x, i.e. averaging over s_0 values in the range $0 \leq s_0 \leq 2\pi R$. The total septum roughness w_{sept} is given by $w(x)$ evaluated at $x=2\pi R$.

To calculate the roughness $w(x)$ averaged over many septum edges, we calculated $w(x)$ of each edge over all length scales $x \leq x_{sat}$ and then grouped length scales into intervals of 80 nm. The roughness measurements were then averaged in each interval. The s.d. of length scales in each interval was too small (~10 nm) to be indicated on the figure.

Estimation of roughness exponent

Power-law fits to roughness were performed using the Curve Fitting Toolbox of MATLAB. The upper limit for the range of scales for the fit was the last increasing data point of $w(x)$. The lower limit of scale for experimental septum edges was the first scale at which roughness was statistically different from zero. The lower limit for simulated septum edges was chosen to be sufficiently larger than the pixel size and the Bgs correlation length a (see supplementary material Table S1).

Derivation of mathematical model of Bgs-mediated septum growth in *S. pombe*

Our model of septum growth proposes that the centripetal force exerted by the contractile ring, which is proportional to local curvature, is communicated to the septum synthesizing apparatus and modifies the local septum growth rate (Fig. 5B). The growth rate of septum at location s on the leading septum edge is given by Eqn 1. The force exerted by the ring of tension T per unit length $\gamma(s,t)$ is proportional to the local curvature $K(s,t)$ of the leading septum edge $\gamma(s,t)=TK(s,t)$. Assuming the rate of change of the slope of h is much larger than h itself ($h \ll R^2\, \partial^2 h/\partial s^2$), the curvature can be expanded to leading order in h and its derivatives as $K(s,t)=1/R-\partial^2 h/\partial s^2$. From these equations, we obtain the spatiotemporal evolution for the ingressing septum edge:

$$-\frac{\partial r}{\partial t}=-\left(\frac{\partial R(t)}{\partial t}+\frac{\partial h(s,t)}{\partial t}\right)=v_{sept}^0+\frac{D}{R}-D\frac{\partial^2 h}{\partial s^2}+\eta_{fluc}(s,t). \quad (4)$$

This gives the basic model equations (see Eqn 2).

The dynamics for the deviation from circularity h of Eqn 2 are similar to the well-studied Edwards–Wilkinson equation (Edwards and Wilkinson, 1982). The scale-dependent roughness $w(x)$ of interfaces that obey Edwards–Wilkinson dynamics varies with the scale of observation according to a power-law with a roughness exponent $\alpha=0.5$ ($w \sim x^{0.5}$), for scales smaller than the system size (Nattermann and Tang, 1992), and for periods of time much longer than a characteristic time scale τ defined by the observation scale x, namely $\tau \sim x^2/D$ (Nattermann and Tang, 1992). This power law growth of roughness is observed up to a characteristic scale x_{sat}

that, initially, grows with time as $x_{sat} \sim \sqrt{Dt}$, until it reaches a value that scales with the size of the system (Nattermann and Tang, 1992).

Simulation of mathematical model of Bgs-mediated septum growth

Using model parameters and the previously measured value of ring tension as input, we developed a stochastic simulation to study septum growth in cells with and without intact rings. We represented the septum edge as a one-dimensional boundary with N evenly spaced points, parameterized by their coordinate ($r_i(t), \theta_i$). These points move inwards in the radial direction as the septum grows inwards. All simulated edges start out as perfect circles with radius R_0 centered at the origin of the coordinate system, unless otherwise mentioned in the text. These N points are initially uniformly spaced with separation $\Delta x_0=(2\pi R_0)/N=40$ nm . The distance between the points decreases as the simulation proceeds. The end of one simulated constriction is defined to be the moment at which a section of the septum leading edge first lies within 20 nm of the origin of the coordinate system, i.e. $\min(r_i(t))=20$ nm.

The contour of the actomyosin ring in the division plane closely follows the contour of the septum edge. The discretized version of Eqn (4) was used for the evolution of the ingressing septum edge, where the local linearized curvature $K_i=(r_{i+1}(t)+r_{i-1}(t)-2r_i(t))/\Delta x^2$.

We used a time step of $\Delta t=10$ ms for the simulation, and the following statistics for the fluctuation in local growth rate:

$$\langle\eta_i(t)\,\eta_{i'}(t')\rangle=\frac{\lambda}{a\tau}f_{ii'}g\left(\frac{|t-t'|}{\tau}\right), \quad (5)$$

where

$$f_{ii'}=\begin{cases}\left(1-\frac{|i-i'|}{M}\right), & |i-i'| \leq M \\ 0, & |i-i'| > M\end{cases}, \quad (6)$$

where $M=a/\Delta x$, and

$$g(x)=\begin{cases}1, & x<1 \\ 0, & x \geq 1\end{cases}. \quad (7)$$

Here, η_i is the growth fluctuation $\eta_{fluc}(s,t)$ from Eqn 4, evaluated at the ith point around the septum edge. The parameters a and τ are a short length and short time scale over which septum growth is correlated, and are related to λ according to $\lambda=v_0^2 a\tau$. The form of the correlation function given in Eqn 5 reduces to $\langle\eta_{fluc}(s,t)\,\eta_{fluc}(s',t')\rangle=\lambda\delta(s-s')\delta(t-t')$ in the continuous limit of vanishing grid size, for $|s-s'| \gg a$ and $|t-t'| \gg \tau$. Simulation parameters are provided in supplementary material Table S1.

Intervals of output time between edges range from 10 s to 130 s. Roughness was extracted from these edges using the same procedure as that used for experimental septum edges. All computational simulations were performed using MATLAB. Scripts can be made available upon request.

Statistical analysis

All quantitative results presented as mean±s.d. or ±95% confidence interval as indicated. Statistical significance was determined using Student's two-tailed t-test for comparison between two independent groups. The 95% confidence intervals for exponents were calculated using the Curve Fitting Toolbox of MATLAB; the confidence intervals for the model parameters D and λ were obtained using chi-squared differences between simulation and experiment (supplementary material Fig. S2C,D).

Competing interests
The authors declare no competing or financial interests.

Author contributions
B.O. designed the research; S.T. and B.O. performed the modeling analysis; E.L.M., R.A. and S.T. performed the experiments; S.T. analyzed the experimental data; T.D.P. provided facilities for experiments; B.O. and S.T. wrote, and T.D.P. edited the paper.

Supplementary material
Supplementary material available online at
http://jcs.biologists.org/lookup/suppl/doi:10.1242/jcs.166926/-/DC1

References

Amir, A., Babaeipour, F., McIntosh, D. B., Nelson, D. R. and Jun, S. (2014). Bending forces plastically deform growing bacterial cell walls. *Proc. Natl. Acad. Sci. USA* **111**, 5778-5783.

Arasada, R. and Pollard, T. D. (2014). Contractile ring stability in S. pombe depends on F-BAR protein Cdc15p and Bgs1p transport from the golgi complex. *Cell Rep.* **8**, 1533-1544.

Balasubramanian, M. K., Srinivasan, R., Huang, Y. and Ng, K.-H. (2012). Comparing contractile apparatus-driven cytokinesis mechanisms across kingdoms. *Cytoskeleton* **69**, 942-956.

Cabib, E. and Arroyo, J. (2013). How carbohydrates sculpt cells: chemical control of morphogenesis in the yeast cell wall. *Nat. Rev. Microbiol.* **11**, 648-655.

Canny, J. (1986). A computational approach to edge detection. *IEEE Trans. Pattern Anal. Mach. Intell.* **8**, 679-698.

Cortés, J. C. G., Carnero, E., Ishiguro, J., Sánchez, Y., Durán, A. and Ribas, J. C. (2005). The novel fission yeast (1,3)beta-D-glucan synthase catalytic subunit Bgs4p is essential during both cytokinesis and polarized growth. *J. Cell Sci.* **118**, 157-174.

Cortés, J. C. G., Konomi, M., Martins, I. M., Muñoz, J., Moreno, M. B., Osumi, M., Durán, A. and Ribas, J. C. (2007). The (1,3)beta-D-glucan synthase subunit Bgs1p is responsible for the fission yeast primary septum formation. *Mol. Microbiol.* **65**, 201-217.

Cortés, J. C. G., Sato, M., Muñoz, J., Moreno, M. B., Clemente-Ramos, J. A., Ramos, M., Okada, H., Osumi, M., Durán, A. and Ribas, J. C. (2012). Fission yeast Ags1 confers the essential septum strength needed for safe gradual cell abscission. *J. Cell Biol.* **198**, 637-656.

Courtemanche, N., Lee, J. Y., Pollard, T. D. and Greene, E. C. (2013). Tension modulates actin filament polymerization mediated by formin and profilin. *Proc. Natl. Acad. Sci. USA* **110**, 9752-9757.

Das, M., Drake, T., Wiley, D. J., Buchwald, P., Vavylonis, D. and Verde, F. (2012). Oscillatory dynamics of Cdc42 GTPase in the control of polarized growth. *Science* **337**, 239-243.

Desai, A. and Mitchison, T. J. (1997). Microtubule polymerization dynamics. *Annu. Rev. Cell Dev. Biol.* **13**, 83-117.

Drake, T. and Vavylonis, D. (2013). Model of fission yeast cell shape driven by membrane-bound growth factors and the cytoskeleton. *PLoS Comput. Biol.* **9**, e1003287.

Edelstein, A., Amodaj, N., Hoover, K., Vale, R. and Stuurman, N. (2010). Computer control of microscopes using μManager. *Curr. Protoc. Mol. Biol. Online* **92**, 14.20.1-14.20.17.

Edwards, S. F. and Wilkinson, D. R. (1982). The surface statistics of a granular aggregate. *Proc. R. Soc. A Math. Phys. Eng. Sci.* **381**, 17-31.

Furchtgott, L., Wingreen, N. S. and Huang, K. C. (2011). Mechanisms for maintaining cell shape in rod-shaped Gram-negative bacteria. *Mol. Microbiol.* **81**, 340-353.

Geertsema, H. J., Kulczyk, A. W., Richardson, C. C. and van Oijen, A. M. (2014). Single-molecule studies of polymerase dynamics and stoichiometry at the bacteriophage T7 replication machinery. *Proc. Natl. Acad. Sci. USA* **111**, 4073-4078.

Hermann, H., Schmidt, P. W. and Schneider, F. (1995). Fractal growth of FeO(OH) during corrosion. *J. Mater. Sci. Lett.* **14**, 816-819.

Jégou, A., Carlier, M.-F. and Romet-Lemonne, G. (2013). Formin mDia1 senses and generates mechanical forces on actin filaments. *Nat. Commun.* **4**, 1883.

Kanbe, T., Kobayashi, I. and Tanaka, K. (1989). Dynamics of cytoplasmic organelles in the cell cycle of the fission yeast Schizosaccharomyces pombe: three-dimensional reconstruction from serial sections. *J. Cell Sci.* **94**, 647-656.

Kardar, M., Parisi, G. and Zhang, Y.-C. (1986). Dynamic scaling of growing interfaces. *Phys. Rev. Lett.* **56**, 889-892.

Kitayama, C., Sugimoto, A. and Yamamoto, M. (1997). Type II myosin heavy chain encoded by the myo2 gene composes the contractile ring during cytokinesis in Schizosaccharomyces pombe. *J. Cell Biol.* **137**, 1309-1319.

Krapp, A. and Simanis, V. (2008). An overview of the fission yeast septation initiation network (SIN). *Biochem. Soc. Trans.* **36**, 411-415.

Lapujoulade, J. (1994). The roughening of metal surfaces. *Surf. Sci. Rep.* **20**, 195-249.

Larson, M. H., Zhou, J., Kaplan, C. D., Palangat, M., Kornberg, R. D., Landick, R. and Block, S. M. (2012). Trigger loop dynamics mediate the balance between the transcriptional fidelity and speed of RNA polymerase II. *Proc. Natl. Acad. Sci. USA* **109**, 6555-6560.

Le Goff, X., Motegi, F., Salimova, E., Mabuchi, I. and Simanis, V. (2000). The S. pombe rlc1 gene encodes a putative myosin regulatory light chain that binds the type II myosins myo3p and myo2p. *J. Cell Sci.* **113**, 4157-4163.

Lesne, A. and Laguës, M. (2012). Growth and roughness of interfaces. In *Scale Invariance: From Phase Transitions to Turbulence*, pp. 259-291. Berlin: Springer-Verlag.

Liu, J., Tang, X., Wang, H., Oliferenko, S. and Balasubramanian, M. K. (2002). The localization of the integral membrane protein Cps1p to the cell division site is dependent on the actomyosin ring and the septation-inducing network in Schizosaccharomyces pombe. *Mol. Biol. Cell* **13**, 989-1000.

Martín, V., García, B., Carnero, E., Durán, A. and Sánchez, Y. (2003). Bgs3p, a putative 1,3-beta-glucan synthase subunit, is required for cell wall assembly in Schizosaccharomyces pombe. *Eukaryot. Cell* **2**, 159-169.

Minc, N., Boudaoud, A. and Chang, F. (2009). Mechanical forces of fission yeast growth. *Curr. Biol.* **19**, 1096-1101.

Muñoz, J., Cortés, J. C. G., Sipiczki, M., Ramos, M., Clemente-Ramos, J. A., Moreno, M. B., Martins, I. M., Pérez, P. and Ribas, J. C. (2013). Extracellular cell wall β(1,3)glucan is required to couple septation to actomyosin ring contraction. *J. Cell Biol.* **203**, 265-282.

Nattermann, T. and Tang, L.-H. (1992). Kinetic surface roughening. I. The Kardar-Parisi-Zhang equation in the weak-coupling regime. *Phys. Rev. A* **45**, 7156-7161.

Pelham, R. J. and Chang, F. (2002). Actin dynamics in the contractile ring during cytokinesis in fission yeast. *Nature* **419**, 82-86.

Pinho, M. G., Kjos, M. and Veening, J.-W. (2013). How to get (a)round: mechanisms controlling growth and division of coccoid bacteria. *Nat. Rev. Microbiol.* **11**, 601-614.

Pollard, T. D. and Wu, J.-Q. (2010). Understanding cytokinesis: lessons from fission yeast. *Nat. Rev. Mol. Cell Biol.* **11**, 149-155.

Proctor, S. A., Minc, N., Boudaoud, A. and Chang, F. (2012). Contributions of turgor pressure, the contractile ring, and septum assembly to forces in cytokinesis in fission yeast. *Curr. Biol.* **22**, 1601-1608.

Roberts-Galbraith, R. H., Chen, J.-S., Wang, J. and Gould, K. L. (2009). The SH3 domains of two PCH family members cooperate in assembly of the Schizosaccharomyces pombe contractile ring. *J. Cell Biol.* **184**, 113-127.

Sparks, C. A., Morphew, M. and McCollum, D. (1999). Sid2p, a spindle pole body kinase that regulates the onset of cytokinesis. *J. Cell Biol.* **146**, 777-790.

Stachowiak, M. R., Laplante, C., Chin, H. F., Guirao, B., Karatekin, E., Pollard, T. D. and O'Shaughnessy, B. (2014). Mechanism of cytokinetic contractile ring constriction in fission yeast. *Dev. Cell* **29**, 547-561.

Stegemann, B., Ritter, C., Kaiser, B. and Rademann, K. (2004). Crystallization of antimony nanoparticles: pattern formation and fractal growth. *J. Phys. Chem. B* **108**, 14292-14297.

Streiblova, E., Hasek, J. and Jelke, E. (1984). Septum pattern in ts mutants of Schizosaccharomyces pombe defective in genes cdc3, cdc4, cdc8 and cdc12. *J. Cell Sci.* **69**, 47-65.

Tebbs, I. R. and Pollard, T. D. (2013). Separate roles of IQGAP Rng2p in forming and constricting the Schizosaccharomyces pombe cytokinetic contractile ring. *Mol. Biol. Cell* **24**, 1904-1917.

Umbach, D. and Jones, K. (2003). A few methods for fitting circles to data. *IEEE Trans. Instrum. Meas.* **52**, 1881-1885.

Ursell, T. S., Nguyen, J., Monds, R. D., Colavin, A., Billings, G., Ouzounov, N., Gitai, Z., Shaevitz, J. W. and Huang, K. C. (2014). Rod-like bacterial shape is maintained by feedback between cell curvature and cytoskeletal localization. *Proc. Natl. Acad. Sci. USA* **111**, E1025-E1034.

Vavylonis, D., Yang, Q. and O'Shaughnessy, B. (2005). Actin polymerization kinetics, cap structure, and fluctuations. *Proc. Natl. Acad. Sci. USA* **102**, 8543-8548.

Wang, L. and Tran, P. T. (2014). Visualizing single rod-shaped fission yeast vertically in micro-sized holes on agarose pad made by soft lithography. *Methods Cell Biol.* **120**, 227-234.

Wang, M. D., Schnitzer, M. J., Yin, H., Landick, R., Gelles, J. and Block, S. M. (1998). Force and velocity measured for single molecules of RNA polymerase. *Science* **282**, 902-907.

Wu, J.-Q. and Pollard, T. D. (2005). Counting cytokinesis proteins globally and locally in fission yeast. *Science* **310**, 310-314.

Zhou, Z., Munteanu, E. L., He, J., Ursell, T., Bathe, M., Huang, K. C. and Chang, F. (2015). The contractile ring coordinates curvature-dependent septum assembly during fission yeast cytokinesis. *Mol. Biol. Cell* **26**, 78-90.